Single and Triple Insulator Tunnel Rectifiers for Infrared Energy Harvesting

S.B. Tekin [1,†], P. Das[2], A.D. Weerakkody[1,*], N. Sedghi[1], S. Hall[1], I.Z. Mitrovic[1,†],
M. Werner[3], J.S. Wrench[3,**], P.R. Chalker[3]
[1]Department of Electrical Engineering and Electronics, University of Liverpool, Liverpool, UK
[2]Dept. of Electronics & Communication Eng., National Institute of Technology (NIT) Durgapur, India
[3]School of Engineering, University of Liverpool, Liverpool, UK

†Corresponding authors: serdar.tekin@liverpool.ac.uk, ivona@liverpool.ac.uk
Current addresses: *Dept. of Electrical, Computer and Energy Eng., University of Colorado, Boulder, USA;
**MDP Co., Applied Materials, UK

Abstract—**Metal Insulator Metal (MIM) and MI^{3}M rectifiers have been fabricated by atomic layer deposition (ALD) to investigate the insulator (Al_2O_3, Ta_2O_5, Nb_2O_5) layer quality and rectification performance for inclusion in rectenna arrays for infrared energy harvesting. ALD has provided superior control of nanometre film thickness (1 to 3 nm) as well as insulator film quality as tunnelling has been found to be the dominant conduction mechanism for all fabricated devices. The Ti/Al_2O_3/Au diode exhibits zero bias responsivity of -0.66 A/W, showing that it can be used for energy harvesting applications without the aid of external bias. Engineering tunnel barriers in non-cascaded (Ta_2O_5/Nb_2O_5/Al_2O_3) and cascaded (Nb_2O_5/Ta_2O_5/Al_2O_3) triple insulator configurations, has been found to shift the onset of rectification reversal from 0.35 V to 1.1 V. A superior low-voltage asymmetry of 6 at 0.1 V and responsivity of 4.3 A/W at 0.35 V are demonstrated for the MI^{3}M diode in non-cascaded configuration.**

Keywords- MIM, rectenna, rectification, ALD, dielectrics

I. INTRODUCTION

Energy harvesting is a promising alternative for sustainable energy generation from renewable sources. Conventional photovoltaic (PV) technology harvests energy in the visible spectrum (400-750 nm), accounting for ~15% of solar radiation and leaving the infrared (IR) range (1-10 μm) fully unexploited. The rectifying antenna (rectenna) is a promising complementary device for capturing this high frequency energy range by collecting it with an antenna and rectifying it into a DC electricity with an integrated rectifier [1-3]. MIM diodes are the best configurations for implementing rectennas in the IR range due to the femtosecond quantum-mechanical tunnelling mechanism [4-6]. For a high-power coupling efficiency, an impedance match between the antenna and the diode ($R_{antenna} = R_{diode}$) is required. This can be achieved by reducing the diode area but this also increases resistance. The trade-off between the resistance (R) and capacitance (C) of the diode is defined by the cut-off frequency determined by the RC time constant [5-8]. The most recent work indicates a possibility of optical rectification through MIM-based rectenna at 28.3 THz (10.6 μm), by using MIM Au/Al_2O_3/Ti [5] and Ti/TiO_2/ZnO/Al MI^{2}M diodes. Although encouraging, the obtained rectenna efficiency is very small (~2.05×10^{-14}) [5] as a result of unoptimized diodes; in the case of both diodes [5, 6], the asymmetry is very low, limiting its rectification ability. For efficient rectification of MIM diodes, there are four important parameters: responsivity ($\beta = dI''(V)/2I'(V)$), asymmetry ($\eta = |I_+/I_-|$ or $|I_-/I_+|$, where I_+ refers to forward bias current and I_- to reverse bias current), dynamic resistance ($R = (dI/dV)^{-1}$) and non-linearity ($f_{NL} = (V/I)\times R$), which can all be derived from experimental current-voltage (I-V) characteristics [1,2].

In this paper, comprehensive experimental and theoretical work is presented on single and triple insulator tunnel diodes with the aim of achieving high asymmetry and zero-bias responsivity for IR rectenna applications. The effect of metal work function difference in the MIM diodes as well as resonant tunnelling (RT) in triple insulator MI^{3}M configurations on the rectification properties has also been studied in detail.

II. DEVICE FABRICATION

MIM devices were fabricated on cleaned ultra-smooth Corning glass plates. The cross-section of fabricated devices and the top view are shown in Fig. 1. The ALD precursors trimethylaluminum (TMA), tantalum ethoxide and niobium ethoxide were used for Al_2O_3, Ta_2O_5 and Nb_2O_5, respectively with H_2O at 140°C precursor temperature. Au, Ti and Al metals were deposited by thermal evaporation. The thickness of the metal electrodes was kept at ~50 nm and the diodes were patterned using a shadow mask having 100 μm×100 μm device area.

The variable angle spectroscopic ellipsometry (VASE) was used to determine thickness, roughness and optical constants (refractive index and extinction coefficient) of the insulator films. The thicknesses are in good agreement with the nominal values depicted in Figs. 1(a)-(d), i.e. (± 0.1 nm) (a)-(b) 3.0 (Al_2O_3), (c) 0.8 (Ta_2O_5)/3.6

$(Nb_2O_5)/1.0$ (Al_2O_3); (d) 1.2 $(Nb_2O_5)/2.4$ $(Ta_2O_5)/1.0$ (Al_2O_3).

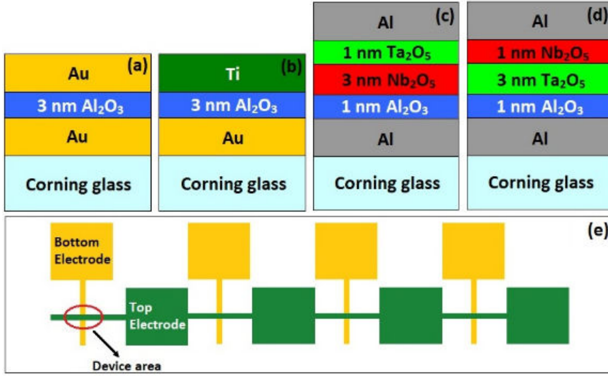

Figure 1. Cross-sections of single (a)-(b) and triple (c)-(d) insulator diodes with varying metal electrodes (Au, Ti, Al); (e) top view of fabricated devices.

III. Results and Discussion

Single and triple insulator MIM diodes were examined by *I-V* measurements performed by a semiconductor parameter analyser integrated with a probe station, at room temperature and under a dark, screened environment. The effect of RT on the *I-V* characteristics of the MI³M diodes is studied using simulations done by in-house MATLAB simulation model [9-11]. Fig. 2 shows *I-V* experimental data on MIM diodes together with extracted rectification parameters of β, R, η and f_{NL}.

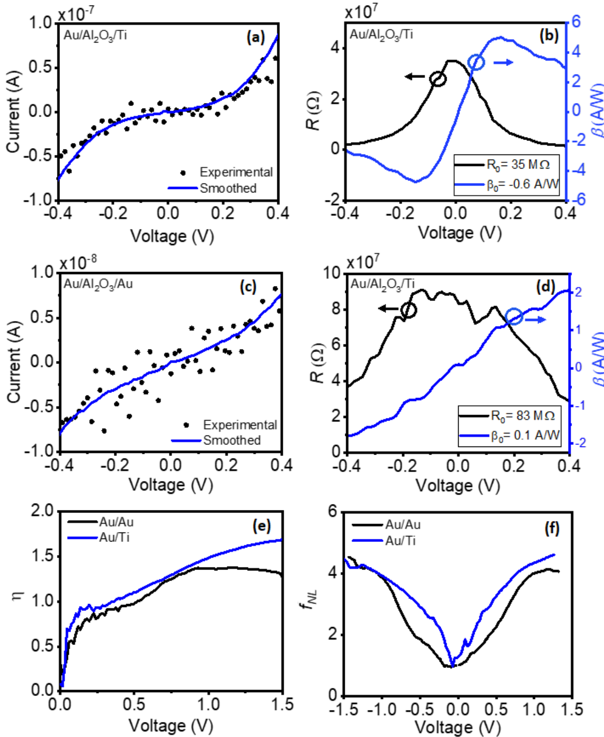

Figure 2. (a)-(f) The *I-V* experimental characteristics with associated extracted rectification parameters R, β, η and f_{NL} for $Au/Al_2O_3/Ti$ and $Au/Al_2O_3/Au$ diodes.

Work function difference has considerable leverage in improving MIM rectification as shown in Figs. 2 (a) and (c). Zero bias resistance (R_0) and responsivity (β_0) of $Au/Al_2O_3/Au$ are found to be 83 MΩ and 0.1 A/W, respectively, while 35 MΩ and -0.6 A/W, respectively for $Au/Al_2O_3/Ti$ diode. The maximum asymmetry values are 1.3 for Au/Au at 1.2 V and 1.7 for Au/Ti diode at 1.5 V. Furthermore, f_{NLmax} at 1.2 V varies from 4.1 for Au/Au to 4.6 for Au/Ti device.

The energy band alignment for non-cascaded and cascaded 1:3:1 triple insulator MI³M configurations was obtained by calculating the voltage division applied across each dielectric film at a given external bias and then determining the number of bound states by MATLAB simulation tool [9]. The energy band diagrams and the possible number of bound states formed in the potential well of the non-cascaded MI³M due to resonant tunnelling for each applied bias are shown in Fig. 3. The oxide parameters, such as dielectric constant and electron affinity as well as metal work function values used in the simulations are summarised in Table 1.

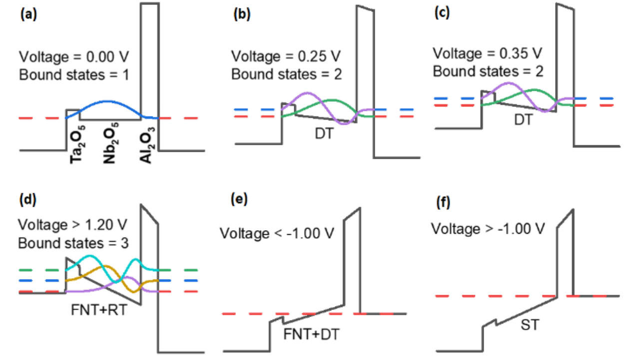

Figure 3. Band line-up for non-cascaded $Ta_2O_5/Nb_2O_5/Al_2O_3$ rectifier with nominal thickness ratio of 1:3:1 under: (a)-(d) positive bias, (e)-(f) negative bias.

Table 1. Summary of material properties used in the simulations of MI³M diode *I-V* characteristics.

Material	Simulation Parameters		
	Dielectric Constant	Electron Affinity (eV)	Work Function (eV)
Al_2O_3	10 [12]	1.60 [12]	--
Ta_2O_5	20 [12]	3.54 [12]	--
Nb_2O_5	25 [12] 40 [13]*	3.72 [12] 4.30 [14]*	--
Al	--	--	4.28 [12]

*These values are used in simulations in Figs. 5 (a) and 7 (a).

It can be seen in Fig. 3 (a) that even when the applied voltage is zero, there is a bound state formed in the conduction band of Nb_2O_5. This is due to the barriers formed at the interfaces of Nb_2O_5 and Ta_2O_5 (0.18 eV), and Nb_2O_5 and Al_2O_3 (2.12 eV) [12]. There is the possibility of having another bound state when the applied bias reaches 0.25 V (Fig. 3 (b)), however there is a very small number of electrons available to tunnel at this energy level due to a large difference between the Fermi level of the metal and the energy level of the bound state. The latter is supported by simulations shown in Fig. 4 (a).

Although there is possibility for resonant tunnelling at two bound states located at 0.51 eV and 0.67 eV, the transmission probability is low (~10^{-11}). However, if the voltage is increased beyond 0.35 V (Fig. 3 (c)), it is possible to observe enhanced current due to resonance or in other words, a relatively larger number of electrons can tunnel via the bound state compared to the case of applied voltage of 0.25 V. This is clearly evident in the transmission and tunnelling probability simulations shown in Fig. 4 (b). The bound states are closer to the Al Fermi level, located at 0.47 eV and 0.63 eV. Also, the transmission probability is higher (~10^{-10}). However, due to the large barrier height between the Al/Nb_2O_5 interface (0.56 eV), a pronounced effect of RT cannot be observed in simulated *I-V* curves in Fig. 5 (a).

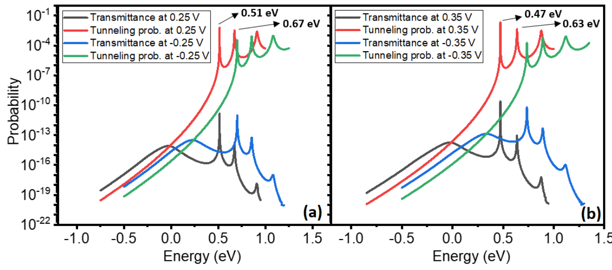

Figure 4. Transmittance and tunnelling probability peaks at (a) ±0.25 V, (b) ±0.35 V and for non-cascaded diode of Al/1.0 nm Ta_2O_5/3.0 nm Nb_2O_5/1.0 nm Al_2O_3/Al.

In Fig. 5 (a), the rectification reversal point (the point where the forward current starts to dominate the reverse due to the RT effect) of the non-cascaded MI^3M diode is observed at ~0.45 V. For further increase of the bias to 1.2 V (Fig. 3 (d)), the Nb_2O_5 layer reaches the Fowler-Nordheim tunnelling (FNT) and RT regimes. The energy difference between the Al Fermi level and three bound states is 0.08 eV, 0.33 eV and 0.59 eV (Fig. 5 (b)). Aligning the Fermi energy of the metal with the bound states gives the maximum transmittance in one direction, and hence the current is enhanced.

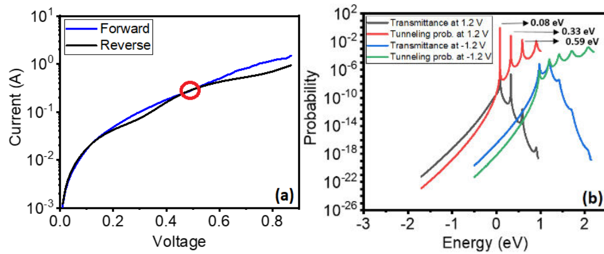

Figure 5. (a) Simulated *I-V* curve, (b) transmittance and tunnelling probability peaks at ±1.2 V for non-cascaded diode Al/1.0 nm Ta_2O_5/3.0 nm Nb_2O_5/1.0 nm Al_2O_3/Al.

For reverse bias, the conduction in the films is dominated by direct tunnelling (DT) when the applied bias is less than -1 V as depicted in Fig. 3(e). A quantum well is created in the conduction band of Nb_2O_5 as the bands are bent. However, as a result of the small barrier between Nb_2O_5 and Ta_2O_5 (0.18 eV), the bound state leaks to the left, resulting in the conduction in reverse bias to be dominated solely by DT and FNT. A potential of ~ -1 V must be applied for the metal Fermi level to overcome the conduction band (CB) of Ta_2O_5 and Nb_2O_5 to reach the step tunnelling (ST) regime (Fig. 3(f)).

The energy band diagrams for cascaded MI^3M structure were produced using the same simulation tool as shown for the previous non-cascaded type. As seen in Fig. 6 (a), no bound states exist in the cascaded structure for zero bias. Fig. 6 (b) illustrates that the conduction process is dominated by DT in all three insulators when the applied bias is < 1.1 V.

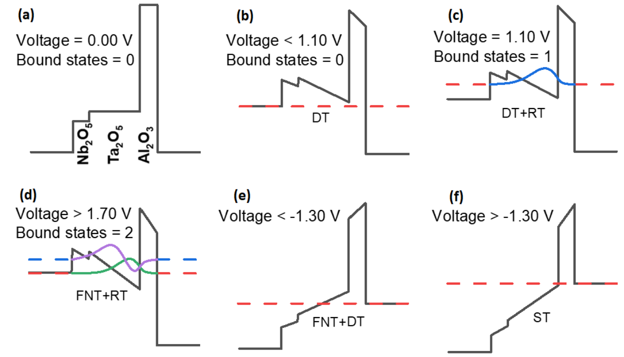

Figure 6. Band line-up for cascaded Nb_2O_5/Ta_2O_5/Al_2O_3 rectifier with nominal thickness ratio of 1:3:1 under: (a)-(d) positive bias, (e)-(f) negative bias.

However, based on electrostatic calculations for the 1:3:1 configuration, beyond 1.1 V, it is possible to obtain a bound state in the conduction bands of both Nb_2O_5 and Ta_2O_5 (Fig. 6 (c)) which could lead to enhanced current due to resonance. The strong resonance is depicted for this structure from 1.7 V (Fig. 6 (d)). For reverse bias, the conduction below -1.3 V is dominated by DT and FNT (Fig. 6 (e)); further increase of voltage beyond -1.3 V leads to a step tunneling regime (Fig. 6 (f)).

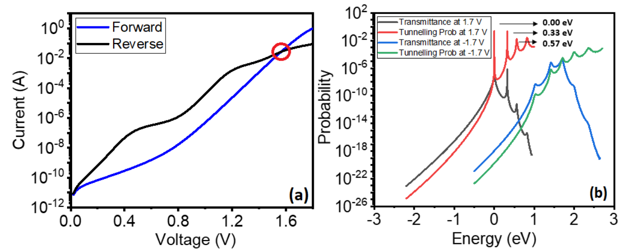

Figure 7. (a) Simulated I-V curve (b) Transmittance and tunnelling probability peaks at ±1.70 V for non-cascaded Al/1.0 nm Nb_2O_5/3.0 nm Ta_2O_5/1.0 nm Al_2O_3/Al.

As shown in Fig. 7 (a), the rectification reversal point is seen at higher voltages ~1.55 V in comparison to non-cascaded configuration. This is due to the variation of oxide thicknesses and configuration. A larger voltage must be applied to increase the depth of the triangular quantum well and a strong effect of RT appears to be evident from 1.7 V as shown in Fig. 7 (b), where the

energy differences between the Al Fermi level and three bound states are 0 eV, 0.33 eV and 0.57 eV.

The experimental rectification characteristics of MI^3M diodes are shown in Fig. 8. Due to differing band alignments of MI^3M configurations, the non-cascaded diode shows a rectification reversal at 0.35 V (Fig. 8(a)), where the forward current starts to dominate reverse current due to the RT and leads to $\eta_{max} = 4.3$ at 1.6 V (Fig. 8 (e)). On the other hand, the rectification reversal for the cascaded diode occurs at a higher bias of ~1.1 V (see Fig. 8 (c)). The latter underpins a large increase in asymmetry of up to ~120 due to RT (Fig. 8 (e), bottom). In the inset of Fig. 8 (e), the $\eta_{max} = |I_-/I_+|$ reaches 6 at 0.1 V.

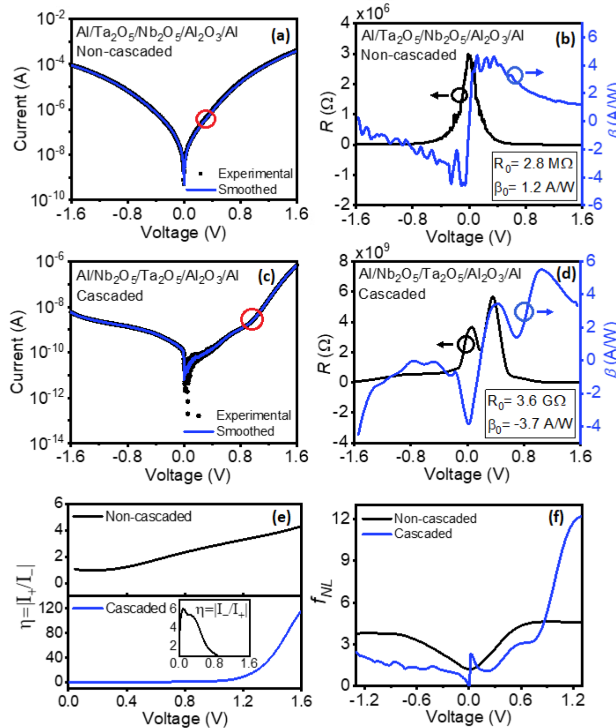

Figure 8. (a)-(f) The experimental I-V curves with associated rectification parameters R, β, η and f_{NL} for MI^3M diodes.

It is worth mentioning that the experimental values of current magnitude and rectification reversal for both MI^3M configurations (Figs. 8 (a), (c)) are smaller than the theoretically predicted ones in Figs. 5 (a) and 7 (a). This could be due to (i) the difference between nominal and actual thicknesses of insulating layers; (ii) the variation in the metal work function of Al, the dielectric constants and the electron affinities of the insulating layers; (iii) the theoretical simulations are only based on the RT mechanism excluding other possible conduction mechanisms. However, the predicted trend in the rectification reversal point increase from non-cascaded to cascaded MI^3M diode is consistent with the experimental results.

Note also an increase in β_0 and f_{NLmax} for both MI^3M non-cascaded and cascaded diodes compared to the MIM diodes. The highest β_0 values of 1.2 A/W and -3.7 A/W were achieved for non-cascaded and cascaded MI^3M diodes, respectively. Also, the maximum responsivity of 4.3 A/W at 0.35 V is demonstrated for the MI^3M diode in non-cascaded configuration. Besides that, the f_{NLmax} for non-cascaded MI^3M is 4.5 at 0.5 V and 11.8 at 1.1 V for the cascaded MI^3M. Furthermore, the R_0 of the non-cascaded and the cascaded structures are 2.8 MΩ and 3.6 GΩ, respectively. This is mainly due to the large barrier heights of 0.74 eV at Al/Ta_2O_5 interface for the non-cascaded configuration, the 3 nm thick Ta_2O_5 and again the large energy barrier of 0.56 eV at the Al/Nb_2O_5 interface. Creating a lower barrier height by fabricating different material interfaces can significantly reduce the device resistance as well as the rectification reversal point can be shifted towards zero-bias.

IV. Conclusion

In summary, the rectification properties (β, η, f_{NL}) of MI^3M diodes are found to be enhanced in comparison to a single M_1IM_2 diode. A fingerprint of resonant tunnelling can be found from a change of curvature and significant increase of current in I-V characteristics. The resonant tunnelling was experimentally observed at 0.35 V for non-cascaded MI^3M device and ~1 V for cascaded MI^3M device. The strong resonant tunnelling effect has an impact on enhanced forward biased current levels and increased asymmetries at higher voltages in all diode structures. The highest low voltage (at 0.1 V) asymmetry and responsivity were observed for non-cascaded MI^3M structure which can be attributed to the effect of direct tunnelling on current transport. Although obtained dynamic resistances of rectifiers are too large for integration with low-resistance antenna part, the results pave the way in further optimising triple insulator configuration by including dissimilar metal electrodes ($M_1I^3M_2$).

Acknowledgement

The EPSRC, UK, EP/K018930/1 and British Council UKIERI F.No.184-1/2018(IC) projects for funding.

References

[1] S. Hall et al., in *Engineering Materials*, Springer, 2014.
[2] G. Moddel and S. Grover, *Rectenna Solar Cells*, pp. 3–24, 2013.
[3] L. Silva et al., *International Microwave and Optoelectronics Conference*, pp. 1–5, 2017.
[4] A.H. Alshehri et al., *Adv. Funct. Mater*., 29, 1805533, 2019.
[5] G. Jayaswal et al., *Materials Today Energy*, 7, pp. 1–9, 2018.
[6] A.Y. Elsharabasy et al., *IEEE J. Photovoltaics*, 9(5), 1232, 2019.
[7] S. B. Herner et al., *IEEE Journal of Photovoltaics,* 8(2), pp. 499–504, 2018.
[8] B. Pelz et al., *Appl. Phys. Lett*., 126, 064503, 2019.
[9] N. Sedghi et al., *Appl. Phys. Lett*., 102, 092103, 2013.
[10] N. Sedghi et al., *in Proceedings of the 43rd ESSDERC*, pp. 131–134, 2013.
[11] I. N. Noureddine et al., *J. Vac. Sci. Tech*., 35, 01A117, 2017.
[12] I.Z. Mitrovic et al., *Appl. Phys. Lett.,* 112, 012902, 2018.
[13] S. Clima et al., *ECS Transactions,*19, pp. 729–737, 2009.
[14] B. Macco et al., *Solar Energy Materials and Solar Cells,* 184, pp. 98–104, 2018.